22nd Australasian Fluid Mechanics Conference AFMC2020
Brisbane, Australia, 7–10 December 2020
https://doi.org/10.14264/5586462

Numerical Simulations of Laboratory–Scale Buoyancy Vortices

T. Bischof[1], M. MacDonald[1], J. E. Cater[2], and R. G. J. Flay[1]

[1] Department of Mechanical Engineering
The University of Auckland, Auckland CBD 1010, New Zealand

[2] Department of Engineering Science
The University of Auckland, Auckland CBD 1010, New Zealand

Abstract

A numerical model was developed using the Unsteady Reynolds–Averaged Navier–Stokes (URANS) method to study the structure, dynamics and flow patterns of buoyancy vortices. Radial vanes and a centrally heated plate produces a buoyancy force for developing a vertical vortex. The effect of grid element size on the accuracy of the numerical model was investigated. In addition, different configurations of heat fluxes and radial vane angles were studied to examine the dynamics of the the vortex. Increases in the maximum temperature and pressure difference occur when the heat flux input is increased. However, the heat flux does not significantly affect the swirl ratio. A 30° vane angle relative to the radial direction led to the highest swirl ratios, while 45° showed the highest temperature and pressure differences. The range of the swirl ratios observed represents a single-cell vortex.

Keywords
Buoyancy vortices, Numerical simulations, CFD, Swirl ratio

Introduction

Buoyancy vortices like dust devils are well-formed low pressure vortices originating from rotating unstable near-surface heated air, and are commonly observed in the turbulent convective boundary layer of the Earth and Mars atmospheres [14]. The width and height of buoyancy vortices range from small (less than a metre wide and a few metres tall) to large (greater than 10 m in width and more than 1000 m tall). The duration and intensity of buoyancy vortices can vary significantly. Dust devils and tornadoes are comparable vortices as both are weather phenomena consisting of a vertically oriented swirling flow. However, tornadoes are much larger and originate from the overlying thunderstorm, while dust devils are mainly generated by local instabilities on the heated ground surface. Most of the available research on buoyancy vortices has focused on structure types, prediction, loading on buildings, property damage or particle movement within vortices, but recently the potential of exploiting the buoyancy vortex kinetic energy to generate power is being investigated(e.g. [4, 5, 7, 13]).

Gaining a better understanding of the origin, the formation process and flow behaviour within buoyancy vortices is of great importance in many fields. Although there have been a few Doppler radar in-field measurements of these flows, the dynamics and flow behaviour of dust devils and tornadoes are complicated. In addition, full-scale and laboratory measurements have limitations related to the duration of the vortex, vortex path, and capturing all aspects of the flow particularly measuring the velocity close to the ground, i.e. below 20 m height in full-scale measurements [9]. Therefore, numerical techniques can be extremely beneficial in simulating and investigating the flow patterns and effects of various parameters on these flows in detail.

Hangan and Kim [3] simulated the structure of a 2D tornado using an unsteady Reynolds–averaged Navier–Stokes (RANS) method and investigated the formation of the vortex. The simulations showed that there is a single to two cell transition, called vortex breakdown, when the swirl ratio, defined in equation (1), is increased to approximately 0.4.

$$S = \frac{u_{tan}}{\overline{w}}, \tag{1}$$

where u_{tan} is the tangential velocity and $\overline{w}$ the vertical velocity. Swirl ratio is a parameter defining the characteristics and intensity of the vortex, and it mostly ranges from 0.2 to 1 [2]. Lower swirl ratios often represent a single-cell vortex, and higher swirl ratios are associated with a two-cell vortex.

Ishihara et al. [6] showed similar results when modelling a Ward-type laboratory vortex chamber using Large-Eddy Simulations (LES). A lower swirl ratio occurs with a one-cell vortex, whereas a two-cell vortex can be obtained by increasing the swirl ratio, which results in a characteristic downdraft in the centre of the vortex. The LES results showed reasonable agreement with the experimental results.

In the first computational study of its kind, Kanak [8] compared LES results of a large scale dust devil with observations, which showed reasonable agreement. In addition the possibility of a vortex formation in the convective boundary layer was investigated and showed a cellular convective pattern with vortex clusters. Kanak's [8] velocity profile of a vortex showed similarities with the analytical Rankine and Burgers–Rott model [10]. Also, other fine scale structures were simulated like spiral bands and inflow jets. The accuracy of such simulations are limited by the near ground boundary conditions and by higher wind speeds which occur often in dust devils.

Natarajan [12] investigated vortex flow characteristics by simulating the Ward-Type Tornado Vortex Chamber and Atmospheric Vortex Engine. Different RANS turbulence models and also LES models were applied to investigate the effects of the surface roughness on the vortex. The k-ε turbulence model was chosen to investigate the available mechanical energy in the Atmospheric Vortex Engine. The results revealed that the main parameter affecting the mechanical energy is the temperature difference between the core and the ambient temperature. Atmospheric stratification was neglected and the model showed limitations in capturing the curvature of the vortex, particularly for higher swirl ratios, which suggests a need for a more accurate approach such as simulations using Reynolds Stress Models or LES.

Natarajan [12] did not study the physics of the vortex and only verified the Atmospheric Vortex Engine concept, and also he did not validate the results. In addition, the effects of vane angles and input heat fluxes on the characteristics of the buoyancy vortices were not investigated.

Due to the complexity of the simulation of buoyancy vortices and in an attempt to develop a more accurate numerical model of buoyancy vortices, this study aims to:

- Numerically model a buoyancy vortex flow based on the experiments carried out by Mullen and Maxworthy [11].
- Investigate the effects of mesh element size on the accuracy of the numerical model. Also validate the numerical model with a previously published experimental study and discuss the discrepancies between the numerical and experimental results, and the potential sources of these differences.
- study the effects of vane configurations and arrangements, and input heat flux on the generated buoyancy vortex.

Methodology

Computational Domain

The geometry and computational domain were selected based on the experimental setup of Mullen and Maxworthy [11]. Figure 1 shows a schematic diagram of the computational domain along with the vanes and a hot plate located at the centre of the box. The box has a cross-section of 3 × 3 m and a height of 2.5 m. The diameter of the hot plate and the height of the vanes are 0.9 m and 1.8 m, respectively.

The effects of various vane angles, relative to the radial direction (namely 30°, 45°, 60°, and 75°) on the velocity and temperature profiles are investigated. In addition, the influence of the input powers of 778, 1058, and 1382 W, corresponding to heat fluxes of 1.2×10^3, 1.6×10^3, and 2.1×10^3 W/m^2, on the flow patterns is also investigated.

The boundary conditions of the computational domain are shown in Figure 1. The input heat flux has a Gaussian distribution and is located at the bottom of the domain from a circular plate. The air at atmospheric conditions enters the domain from the bottom periphery of the domain through a 0.3 m high gap. Lastly, the vortex exits from the top of the domain at ambient conditions.

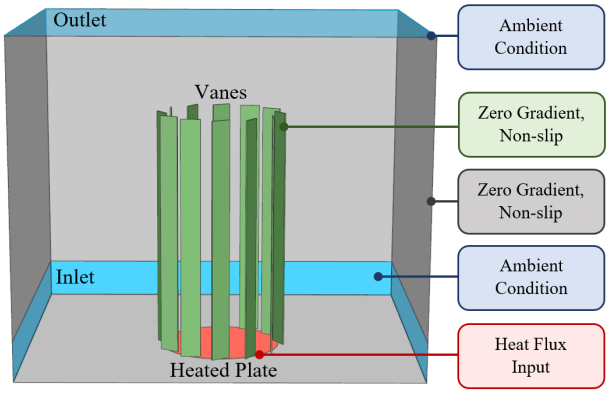

Figure 1. Boundary conditions of the computational domain.

Computational Mesh

OpenFOAM software with a user-defined method, called SnappyHexMesh, was used to generate mesh elements in the computational domain. The elements are predominately hexahedral, particularly far from the vanes. At the centre of the domain and around the vane surfaces a much finer mesh was generated, where at some locations tetrahedral elements were required to ensure the vane geometry was resolved.

A mesh dependence study was conducted out using the method proposed by Celik et al. [1], that determines the grid-convergence index (GCI). For this purpose, three different grid sizes with a total number of elements of approximately 50, 20, and 6 million, corresponding to average cell sizes of 0.0077 m, 0.0103 m, and 0.0153 m, were used. As recommended by Celik et al. [1], the grid-refinement factor was maintained greater than 1.3. In addition, iterative convergence was achieved by ensuring that the residuals were at least below 10^{-6}. The values of velocity and temperature across the radius of the vortex obtained from the three grid sizes along with the corresponding error values are reported in the Results section.

Numerical Method

The 3D, transient, non-isothermal simulation was conducted utilising the open-source, OpenFOAM software by solving the RANS equations. For this preliminary study, only the k-ε turbulence model was used to evaluate its performance in modelling the buoyancy vortices and to compare with experimental results. For both advection and turbulence terms of the governing equations, the first-order upwind scheme was used.

Results and Discussion

Mesh Dependency Investigation

The numerical simulation was carried out with three grid sizes, fine (N1), medium (N2) and coarse (N3) for a power input of 778W and vane angle of 45°. To investigate mesh dependency, the value of the swirl ratio S, (equation (1)), for each grid size was obtained, and by using S, the apparent order of accuracy (p) of the numerical method, extrapolated value ϕ_{ext}^{21}, and relative errors (e_a^{21} and e_{ext}^{21}) were computed and are reported in Table 1.

N1 / N2 / N3		49,160,672 / 20,872,660 / 6,326,064		
ϕ_1 / ϕ_2 / ϕ_3		0.091 / 0.103 / 0.111		
r_{21} / r_{32}		1.33/ 1.49		
p	ϕ_{ext}^{21}	e_a^{21}	e_{ext}^{21}	GCI_{fine}^{21}
3.53	0.084	12.99%	8.06%	9.32%

Table 1. Grid-Sensitivity Analysis for swirl ratio (S) [1].

First-order discretisation schemes were used for the present simulations. However, as can be seen in Table 1, the calculated p value is 3.53. According to Celik et al. [1] when either of ε values are very close to zero, the procedure provided for calculating p does not work. However, it is not a sign of unsatisfactory calculations [1].

The relative approximate error, relative extrapolated error and GCI between the results of the fine and medium grids are around 13%, 8%, and 9% respectively, and these are within an acceptable range. As the relative error between the medium and fine mesh is very low, the results from the medium grid have been used for the further analysis.

Validation

Profiles of the radial temperature difference from ambient (ΔT) across the vortex at three different heights and three power inputs obtained were compared with the experimental results of Mullen and Maxworthy [11]. Reasonable agreement was

achieved between the numerical and experimental results. Figure 2 compares the numerical and experimental results of the radial temperature profiles for a input power of 778 W and a vane angle of 45°. The plot is normalised by the ambient temperature of 294.15 K and the radius R of the hot plate.

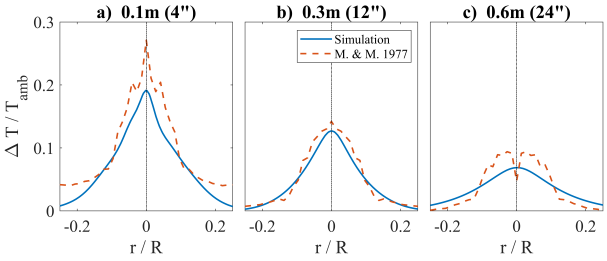

Figure 2. ΔT comparison between numerical model and experiment at different heights [11].

Both the experimental and numerical results show a decrease in temperature difference with height, with a peak at the vortex core. Mullen & Maxworthy [11] measured a slightly higher peak and steeper temperature gradients. These differences could be due to the measurement techniques and experimental errors, and also the modelling assumptions. In addition, the experiment introduced suction at the top of the domain which was not modelled numerically.

Effects of Heat Flux and Vane Angle

The effects of the input power and the vane angle on the flow pattern were investigated using three different input powers (778W, 1058W, 1382W) and four vane angles (30°, 45°, 60°, and 75°). The patterns of four parameters, namely (ΔT), pressure difference from ambient (Δp), tangential and vertical velocities (u_{tan} and w), across the vortex at three different heights under the 12 cases, were investigated.

Figure 3 shows the trend of these parameters across the vortex for power and vane angle of 778W and 45° respectively at three different heights.

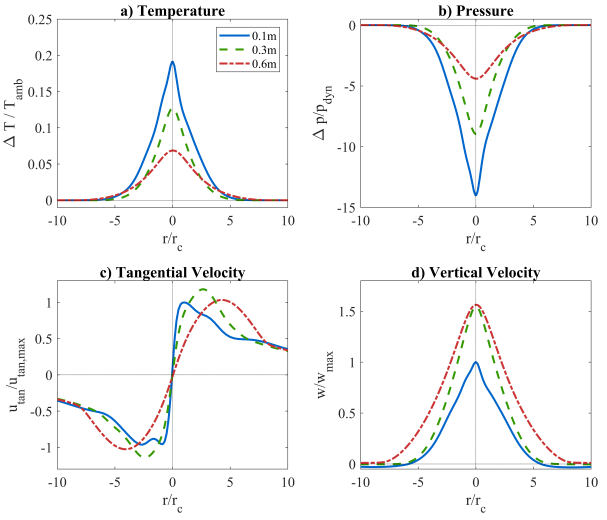

Figure 3. Temperature difference, pressure difference, tangential and vertical velocities across the vortex at a power and vane angle of 778W and 45°, respectively.

The temperature is non-dimensionalised again by the ambient temperature and the velocities by their maximum values $u_{tan,max}$ and w_{max} at 0.1 m height. The pressure is non-dimensionalised by the dynamic pressure $p_{dyn} = 0.5 * \rho * w_{max}^2$ using the maximum vertical velocity at 0.1 m height. The radius is normalised by the core radius r_c which is the radial position where the maximum tangential velocity occurs.

In Figures 3(a,b,d), there is only one peak in the ΔT, Δp and w profiles at the vortex centre, which represents a single-cell vortex structure. As the height increases, both ΔT and Δp (Figures 3 a,b) decrease. On the other hand, the vertical velocity increases further away from the heat source. At higher elevations, the tangential velocity peak occurs farther from the vortex core, showing that the vortex core expands with the height.

In addition, the tangential velocity u_{tan} at 0.3m height can be compared to known analytical and empirical models [10], as can be seen in Figure 4. The normalised tangential velocity profile of the computed k-ε model has a similar shape to the Rankine and Sullivan Model outside the vortex core, $r > r_c$. However, around the peak and inside the vortex core, $r < r_c$, the tangential velocity profile seem to follow a more realistic-advanced model, such as the Burgers-Rott and the Bjerknes Model.

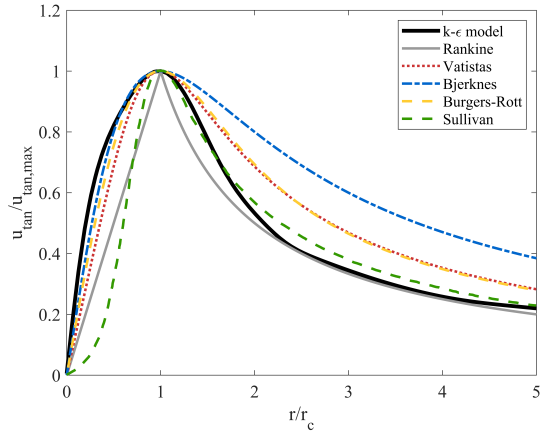

Figure 4. Tangential velocity profiles of the numerical result at 0.3 m height and the analytical and empirical models[10]

To further investigate the influence of the input power and vane angle on the flow parameters, Figure 5 depicts the maximum ΔT, Δp, and the swirl ratio (calculated using equation (1) with the maximum tangential velocity and averaged vertical velocity) in the vortex core at 0.3 m above the ground.

As can be seen, increasing the input power considerably increases the maximum ΔT and Δp, while the input power has little effect on the swirl ratio. Vane angles of 45° and 75° resulted in higher ΔT and Δp, with 45° vane angle generating slightly larger ΔT and Δp, particularly at higher input powers. Even though the changes are not significant, it is clear that a vane angle of 30° results in the lowest maxima. This higher pressure differences imply a stronger vortex which can also be seen in the swirl ratio. When considering the vane angle influence on the swirl ratio, the 30° and 75° vane angles produce the highest and lowest swirl ratios, respectively.

The computed swirl ratios from the numerical model show a range from 0.02 to 0.16. As mentioned, lower values often represent a single-cell vortex [2], which is also in agreement with the single peaks observed in the profiles of ΔT and Δp.

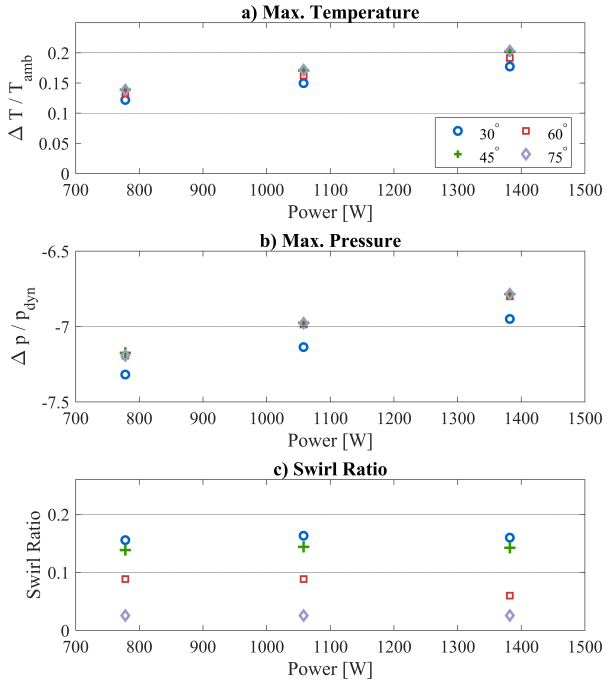

Figure 5. Maximum ΔT, Δp and Swirl ratio for 12 configurations.

Conclusions

A 3D, transient, non-isothermal numerical model using the k-ε RANS turbulence model was developed to simulate laboratory-scaled buoyancy vortices. Reasonable agreement was obtained between the simulation results and the experimental results of Mullen and Maxworthy [11]. The numerical simulations were conducted using three different grid sizes to evaluate the accuracy of the developed model. Several analytical vortex models of the tangential velocity were compared with the present numerical results, which showed excellent agreement with the Rankine and Burgers-Rott models. The effects of different input heat fluxes and vane angles on the flow pattern and various parameters of the buoyancy vortices, including the temperature and pressure differences, and tangential and vertical velocities, were investigated in detail. It is demonstrated that an increase in the input heat flux considerably increases the temperature and pressure differences, while it has a negligible effect on the swirl ratio. On the other hand, the vane angles significantly influence the swirl ratio, with the 30° vane angle producing the highest swirl ratio. The computed configurations with vane angles of 45° and 75° resulted in higher temperature and pressure differences.

In future work, higher-resolution schemes and finer grid sizes will be employed to verify the simulation accuracy. In addition, different turbulence models, e.g. k-Ω and SST k-Ω, will be used.

Acknowledgements

The authors acknowledge the financial support from the Royal Society Te Apārangi of New Zealand for the Marsden Fund grant 18-UOA-013, entitled “Reap the Whirlwind and Produce Carbon-Neutral Power From Atmospheric Buoyancy Vortices”. The authors wish to acknowledge the use of New Zealand eScience Infrastructure (NeSI) high performance computing facilities, consulting support and/or training services as part of this research.

References

[1] Celik, I. B., Ghia, U., Roache, P. J., Freitas, C. J., Coleman, H., and Raad, P. E. (2008). Procedure for Estimation and Reporting of Uncertainty Due to Discretization in CFD Applications. *J. Fluids Eng.*, 130(7), 078001 (DOI: 10.1115/1.2960953).

[2] Church, C. R., Snow, J. T., Baker, G. L., and Agee, E. M. (1979). Characteristics of Tornado-like vortices as a function of swirl ratio: a laboratory investigation. *J. Atmos. Sci.*, 36, 1755–1776 (DOI: 10.1175/1520-0469(1979)036¡1755:COTLVA¿2.0.CO;2).

[3] Hangan, H. and Kim, J-D. (2006). Numerical Simulation of Tornado Vortices. *The 4th International Symposium on Computational Wind Engineering*. CWE2006, Yokohama, Japan.

[4] Hawkes, N. (2016). Reaping the Whirlwind: Buoyancy Vortices as Virtual Chimneys for Power Generation from Waste Heat. *Master Thesis*, University of Auckland, Auckland, New Zealand.

[5] Hawkes, N. and Flay, R. G. J. (2016). A Model of Tangential Windspeeds in Dust Devils. *9th Asia-Pacific Conference on Wind Engineering*. Auckland, New Zealand.

[6] Ishihara, T., Oh, S. and Tokuyama, Y. (2011). Numerical study on flow fields of tornado-like vortices using the LES turbulence model. *J. Wind E. Ind. Aerodyn.*, 99, 239–248 (DOI: 10.1016/j.jweia.2011.01.014).

[7] Ismaeel, A. A., Al-Kayiem, H. H., Baheta, A. T. and Aurybi, M. A. (2017). Review and comparative analysis of vortex generation systems for sustainable electric power production. *IET Renew. Power Gener.*, 11(13), 1613–1624 (DOI: 10.1049/iet-rpg.2017.0058).

[8] Kanak, K. M. (2005). Numerical simulation of dust devil-scale vortices. *Q. J. R. Meteorol. Soc*, 131, 1271–1292 (DOI: 10.1256/qj.03.172).

[9] Kashefizadeh, M. H., Verma, S. and Selvam, R. P. (2019). Computer modelling of close-to-ground tornado windfields for different tornado widths. *J. Wind Eng. Ind. Aerod.*, 191, 32–40 (DOI: 10.1016/j.jweia.2019.05.008).

[10] Kim, Y. C. and Matsui, M. (2017). Analytical and empirical models of tornado vortices: A comparative study. *J. Wind Eng. Ind. Aerod.*, 171, 230–247 (DOI: 10.1016/j.jweia.2017.10.009).

[11] Mullen, J. B. and Maxworthy, T. (1977). A laboratory model of dust devil vortices. *Dynam. Atmos. Oceans*, 1, 181–214 (DOI: 10.1016/0377-0265(77)90006-9).

[12] Natarajan, D.(2011). Numerical Simulation of Tornado-like Vortices. *PhD Thesis*, University of Western Ontario, Ontario, Canada.

[13] Nizetic, S. (2011). Technical utilisation of convective vortices for carbon-free electricity production: A review. *Energy*, 36(2), 1236–1242 (DOI: 10.1016/j.energy.2010.11.021).

[14] Reiss, D., Raack, J. and Hiesinger, H. (2011). Bright dust devil tracks on Earth: Implications for their formation on Mars. *Icarus*, 211(1), 917–920 (DOI: 10.1016/j.icarus.2010.09.009).